





# A zeolite crystallisation model confirmed by *in situ* observation†

Nick Pellens, <sup>a</sup> Nikolaus Doppelhammer, <sup>ac</sup> Karel Asselman, <sup>a</sup>  
Barbara Thijs, <sup>a</sup> Bernhard Jakoby, <sup>c</sup> Erwin K. Reichel, <sup>c</sup>  
Francis Taulelle, <sup>ab</sup> Johan Martens, <sup>ab</sup> Eric Breynaert <sup>ab</sup>  
and C. E. A. Kirschhock <sup>\*a</sup>

Probing nucleation and growth of porous crystals at a molecular level remains a cumbersome experimental endeavour due to the complexity of the synthesis media involved. In particular, the study of zeolite formation is hindered as these typically form in multiphasic synthesis media, which restricts experimental access to crystallisation processes. Zeolite formation from single phasic hydrated silicate ionic liquids (HSiL) opens new possibilities. In this work, HSiL zeolite crystallisation is investigated *in situ* using a specifically designed conductivity measurement set-up yielding access to crystallisation kinetics. Based on the conductivity data and final yields, a crystallisation model explaining the results based on a surface growth mechanism was derived. The excellent agreement between experiment and theory indicates zeolite crystallisation from highly ionic media proceeds *via* a multi-step mechanism, involving an initial reversible surface condensation of a growth unit, followed by incorporation of that unit into the growing crystal. The first step is governed by the liquid phase concentration and surface energy, while the final step shows a correlation to the mobility of the cation involved.

## 1. Introduction

Classical nucleation theory (CNT) describes the stochastic condensation of atoms, ions, and molecules into an ordered lattice.<sup>1</sup> While it successfully explains the formation of many simple crystals, a score of crystalline materials crystallise *via* more complex multi-step mechanisms involving metastable intermediates, such as oligomers, complexes, the initial formation of an emulsion of a dense liquid in a solvent, or amorphous and crystalline nanoparticles.<sup>2</sup> Indeed, experimental observations clearly show that molecular-scale processes during crystal

---

<sup>a</sup>KU Leuven, COK-KAT, Leuven, Belgium. E-mail: christine.kirschhock@kuleuven.be

<sup>b</sup>KU Leuven, NMRCoRe, Leuven, Belgium

<sup>c</sup>JKU Linz, Institut für Mikroelektronik und Mikrosensorik, Linz, Austria

† Electronic supplementary information (ESI) available. See DOI: 10.1039/d1fd00093d

nucleation and growth need to be accounted for. Magnetite, for example, can nucleate both *via* ordered or non-ordered intermediates, depending on the relative thermodynamic (meta)stability of these units in the system.<sup>3</sup> Interestingly, condensation of these precursors follows a kinetic regime reminiscent of colloidal assembly,<sup>4</sup> disregarding differences between surface energies of crystal facets. Also, calcium carbonates and calcium phosphates can nucleate *via* the condensation of solute pre-nucleation clusters,<sup>5-7</sup> which for calcium phosphate can be related to ion-association complexes.<sup>7</sup> To account for such complex multistep mechanisms, CNT has been extended with modern nucleation theory. But even here, perceived initial states and growth units are often described with thermodynamic properties of the bulk, owing to the limited mechanistic insight into crystal growth.<sup>1</sup> Crystallisation kinetics usually are evaluated *via* DSC, XRD, TEM or NMR, and data interpretation is often quite limited by the signal-to-noise ratio.<sup>8</sup> Accurate description of crystallisation, however, critically depends on models integrating the chemistry and energetics of the specific system in detail.<sup>8,9</sup> Unfortunately, molecular-level observation of growth processes is difficult and requires advanced *in situ* diagnostics.<sup>10,11</sup>

Zeolite nucleation is a striking example. Insight into early zeolite formation is hindered by the sol-gel nature of common zeolite synthesis media.<sup>10</sup> Despite these limitations, several attempts have been made to formulate general scenarios,<sup>10,12-15</sup> hypotheses ranging from classical amorphous densification to non-classical crystallisation *via* precursor attachment involving oligomers up to nanocrystals.<sup>2,16</sup> To experimentally access molecular steps of zeolite formation, simplified zeolite synthesis media and/or a step change in diagnostics are required.

The discovery of zeolite formation in monophasic hydrated silicate ionic liquids (HSiLs) provides opportunities to study zeolite crystallisation in more detail.<sup>17</sup> HSiLs are entirely inorganic, homogenous liquids composed of hypolvated silicate oligomers and alkali hydroxides. They allow the study of zeolite formation on a molecular level<sup>18</sup> and thereby may aid the advance of modern nucleation theory in general.<sup>19</sup> Within HSiLs, zeolite formation is initiated by pre-nucleation cluster consisting of ion pairs of soluble aluminosilicate oligomer anions with alkali cations.<sup>19</sup> When the chemical conditions in the liquid favour formation of such ion pairs, ordered assembly into a zeolite phase is observed.

Insight in kinetics and rate-limiting steps of crystal nucleation and growth is essential to control crystal morphology, size, and eventually topology. In hypo-hydrated conditions, negatively charged deprotonated silanol functions prevent disordered silicate condensation into amorphous phases, and inner sphere ion-pairing of aluminosilicate oligomers with alkali cations into pre-nucleation clusters is observed. Ordered assembly of these pre-nucleation clusters into a zeolite phase implies the removal of the negative charge by nucleophilic substitution reactions, generating hydroxide ions as leaving groups.<sup>19</sup> These hydroxide ions, along with charge-compensating cations, are released into the crystallisation medium. This increases the conductivity of the synthesis liquid as zeolite crystallisation proceeds, providing experimental access to the progressing crystallisation *in situ*. In the absence of amorphous phases or dissolving framework sources, the increase in conductivity must show a linear relationship with every additional siloxation in the medium, providing a direct correlation between zeolite crystallisation and accurate *in situ* conductivity measurements. Discovery

of ion-paired pre-nucleation clusters in zeolite crystals is in full agreement with the theory describing magnetite precipitation, a model entirely based on thermodynamic arguments.<sup>3</sup>

In this work, it will be shown that the interaction strength of the cation with the pre-nucleation cluster and crystal surface determines crystal morphology and size, allowing rationalisation and control of the formation of zeolites, and by extension, complex materials in general. With the discovery of zeolite pre-nucleation clusters, modern nucleation theory can now also adequately describe zeolite formation. Adding zeolites to the list of minerals for which nucleation is explained with a similar level of detail as has been possible for calcium carbonate and phosphate,<sup>5</sup> holds promise that the documented approach here will inspire researchers to add many more complex porous crystals to the list of crystallisation systems explained by modern nucleation theory.

## 2. Experimental details

HSiL synthesis liquids with molar composition 0.5 Si(OH)<sub>4</sub>:0.03 Al(OH)<sub>3</sub>:1 MOH:5 H<sub>2</sub>O were prepared in the presence of sodium or cesium hydroxide (M = Na<sup>+</sup> or Cs<sup>+</sup>) and stirred for 24 h at room temperature (details in ESI†). Zeolites were crystallised from the synthesis liquids at temperatures of 60, 70, 80, and 90 °C. During synthesis, conductivity was measured *in situ* by MEEIS, using a custom measurement cell (Fig. S1†). HSIL zeolite synthesis liquids were loaded into the preheated cell after being stirred for 24 h at room temperature, achieving fast thermal equilibration times of <10 min with  $\Delta T < 0.01$  °C. To inhibit evaporation, the moveable electrode was tightly sealed by a silicone cap. Impedance spectra were measured at 13 electrode distances between 5 and 9 cm. For each electrode distance, impedance values at 30 logarithmically spaced frequencies were recorded in the range of 10 Hz to 1 MHz, in two-electrode potentiostatic mode, using a peak-to-peak amplitude of 0.1 V. Conductivity sampling times of 7 and 30 minutes were chosen for fast and slow crystallising samples, respectively. Samples were monitored until the conductivity curve plateaued. Zeolite syntheses were replicated in synthesis liquid from the same batch as used for *in situ* conductometry (details in ESI†). The recovered solids were collected, washed *via* repeated dispersion–centrifugation (15 min, 35.000g), and studied with powder X-ray diffraction (PXRD) and scanning electron microscopy (SEM). PXRD patterns (CuK<sub>α1</sub>) were recorded on a STOE STADI P Combi diffractometer in high-throughput mode, with a curved image plate PSD and focusing Ge(111) monochromator. High resolution SEM images were recorded with a Nova NanoSEM450 (Fei, Hillsboro, OR).

## 3. Results

### 3.1 Product characterisation

According to PXRD measurements (Fig. 1) and SEM images (Fig. 2) all synthesis products are zeolitic, being of ANA topology for all Cs-containing samples. The Na syntheses yielded mixtures of FAU, GIS and SOD, with increasing GIS fractions at higher temperature. SEM revealed significant differences in crystal size and morphology of the synthesis products. All Cs samples show nearly identical isotropic morphologies of 100–200 nm crystal sizes. Note that during synthesis,

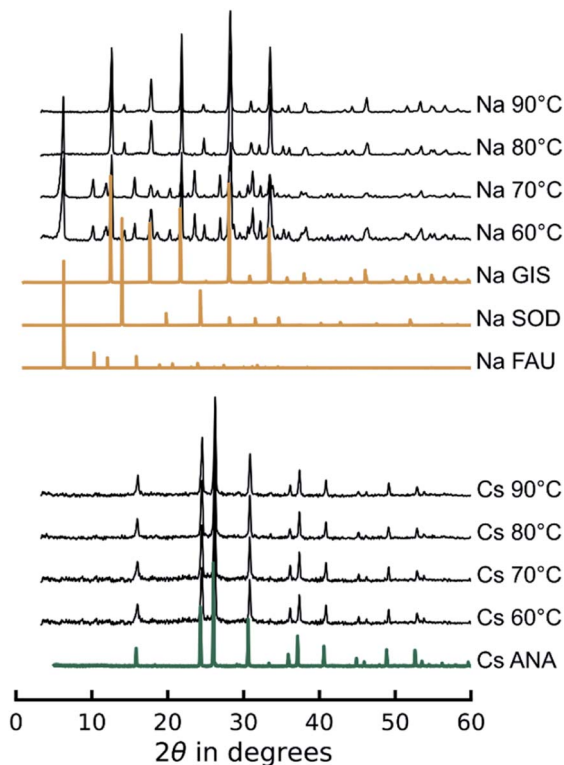


Fig. 1 X-ray diffraction measurements of the synthesis products. Synthesis liquids containing Na cations yielded mixtures of the GIS/FAU/SOD zeolites. Zeolite synthesis in the presence of Cs cations yielded a phase-pure ANA zeolite in all cases. The sample labels indicate a synthesis liquid either containing Na or Cs cations, synthesized at temperatures of 60, 70, 80 or 90 °C.

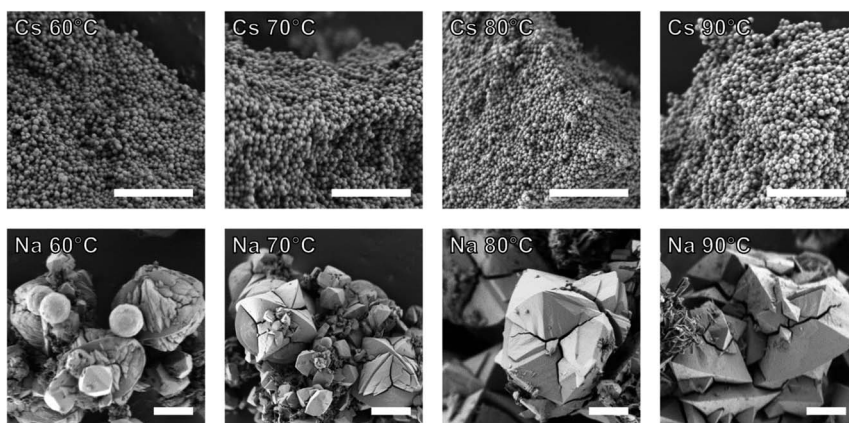


Fig. 2 Scanning electron microscopy imaging of the synthesis products. The white markers represent 2 μm in all figure frames. Images were selected to be representative of the studied samples.

these spheres are isolated and aggregate only during product recovery. Crystals of the Na samples are more than an order of magnitude larger and crystal morphology strongly depends on synthesis temperature. At low temperatures, the crystals show emerging crystal facets, but are partly spherical. Increasing synthesis temperature defines the facets more clearly, while overall crystal size increases. An earlier study on the crystallisation kinetics of MER in K systems yielded a similar result.<sup>20</sup> These observations suggest zeolite nucleation and crystal growth to be strongly affected by crystallisation kinetics.

### 3.2 Modelling of the conductivity curves

All *in situ* conductivity curves show sigmoidal behaviour, strongly dependent on temperature and cation type (Fig. 3). The plateaus of the curves were used to define the synthesis time ( $t_{\text{final}}$ , Table S1†) as the time where no further formation of zeolite material is detected. To analyse the measured conductivity in terms of crystallisation, a model describing the global zeolite content of the liquids as a function of time is necessary. For this, the growth of all observed zeolite phases, irrespective of topology, is considered to proceed *via* ion-paired pre-nucleation clusters involving surface condensation and release of metal hydroxide to the synthesis liquid, which relates to the measured change of conductivity,<sup>19</sup>

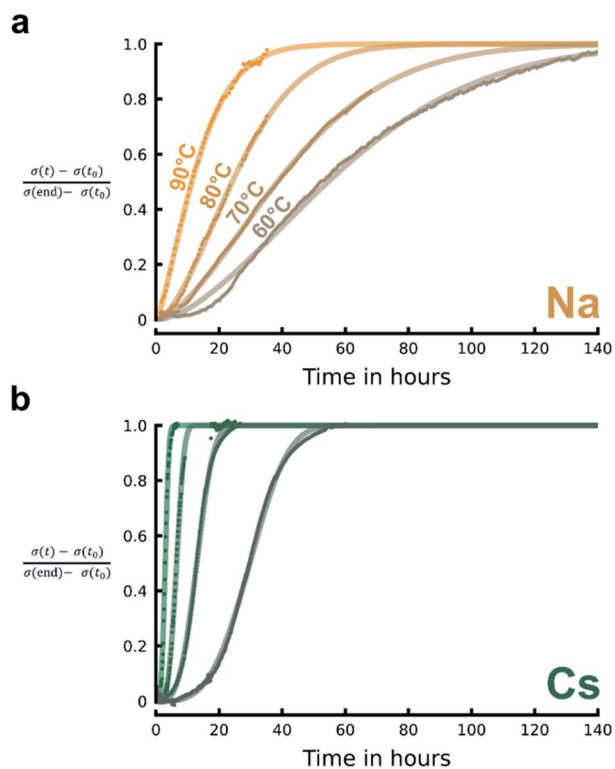


Fig. 3 MEEIS conductivity measurements. (a and b) Conductivity curves of samples containing Na and Cs cations, respectively. Measured data is given by point markers. The best fit is given by the line markers (details in ESI†).

$$\frac{\text{Solid product } (t)}{\text{Total solid product } (t_{\text{final}})} \propto \frac{\sigma(t) - \sigma(t_0)}{\sigma(t_{\text{final}}) - \sigma(t_0)}$$

**3.2.1 Liquid phase chemistry.** Composing the synthesis mixture, aluminate is added to a purely siliceous HSIL, followed by stirring at room temperature for 24 h. Aluminate is consequently incorporated into aluminosilicate oligomers which are all in chemical equilibrium. As a result, Al can be assumed to always be homogeneously distributed over the silicate oligomers in the liquid, including the pre-nucleation clusters.<sup>18</sup> In the liquid, negative charges arising from deprotonated silanol and aluminol groups are compensated by alkali cations, the nature of the cation determining the interaction strength in the ion pair. In the hypo-hydrated conditions governing the synthesis medium, cations complete their coordination sphere with aluminosilicate oligomers. This results in a dense network of interlinked coordination polyhedra reminiscent of what is observed in highly concentrated sub-hydrated alkali hydroxides.<sup>18,21</sup> Assuming rapid interaction kinetics in the polyhedral network, each species, including viable pre-nucleation clusters, are available in any volume element of the synthesis medium. Therefore, upon heating, nucleation occurs at random within the total volume of the network.

**3.2.2 Model of increasing zeolite fraction.** The conductivity data acquired reflects the increasing fraction of zeolite, assuming the volume and the chemical state of the liquid fraction does not change significantly. This leads to a quasi-linear relation between conductivity increase and solid phase formation. Since silica-gelation is prevented by the high charge density of the clusters and the absence of a bulk solvent phase, at the start of the crystallisation the studied systems do not contain any solids. During the experiment, only the formation of crystalline zeolitic material is observed, indicating zeolite formation occurs as result of the limited solubility of the aluminosilicate oligomers in the concentrated alkali metal hydroxide liquid. As zeolite formation is correlated to the removal of pre-nucleation clusters (PNC) from the liquid, the relation between solid and liquid phase can be described with a very simple microscopic picture.

Considering a set of assumptions, a statistical model describing the probability for a PNC to have crystallised can be formulated. First it is assumed that any PNC in the vicinity of a growing crystal will attach, as long as the concentration  $c$  exceeds the liquid-state solubility limit  $c_s$ : ( $c - c_s > 0$ ) implies PNC attachment. Based on this assumption, the focus can be shifted to the number of liquid-state PNCs, which, at the end of the reaction, have been incorporated into zeolite crystals. This number is a direct function of the initial supersaturation ( $N_0 - N_s = V_{\text{liquid}}(c(t_0) - c_s)$ ). Inspecting the morphology of the products (Fig. 2), 3D growth is evident, *i.e.*, it is assumed that the volume of the crystals can be described by a cubic function of their effective radius. With these considerations, the description of these systems can be simplified further. If the number density of PNC exceeds solubility, zeolite will form with nucleation and growth rates characteristic for the growing crystals.<sup>1</sup> This allows the product fraction at a time  $t$  to be used as an expression describing crystallisation progress. To allow comparison between systems, irrespective of cation and formed topology, several additional simplifications are made: (1) at each time, the system consists of a small fraction of growing crystals in the presence of abundant liquid growth medium, such that the liquid volume can be considered

constant. (2) Kinetics and dynamics in the liquid medium are fast, implying chemical equilibrium in the liquid throughout the crystallisation. This implies that every species relevant for crystal growth is always available within any volume fraction of the liquid medium, and crystal growth is rate-limited by processes occurring on the crystal surface. (3) Crystal growth proceeds until the solubility of the growing phases ( $c_s$ ) is reached, *i.e.*  $c(t_{\text{final}}) - c_s = 0$ . (4) For a given cation and synthesis temperature, the growth mechanism does not change. (5) Surface processes are similar for all surfaces and phases growing at the same moment, and total yield is defined by the total solid obtained at  $t_{\text{final}}$ .

Considering  $N_0$  to be the total number of PNC present at time zero in a constant liquid volume  $V_{\text{liquid}}$  (assumption 1), at  $t_{\text{final}}$ ,  $N_c (=N_0 - N_s)$  PNCs have transformed into the solid.  $N_c$  thus represents the number of PNC exceeding the solubility in  $V_{\text{liquid}}$  and  $(c(t_0) - c_s) > 0$  (assumption 3). This averages supersaturation over all growing phases so that phase transformations are currently not explicit in this model. Instead, only the time-dependent increase of total zeolitic material is considered. Assuming fast liquid-phase kinetics and dynamics (assumption 2), it is now possible to determine a probability for the progress of crystallisation. In the liquid, all PNCs in the population  $N_c$  are in constant exchange with all oligomeric species, so that the statistical model can be reduced to the conversion of  $N_c$  PNCs into crystalline solid. The increasing crystal fraction in time thus determines the probability that a PNC of population  $N_c$  has already crystallised. Identifying the volume increase of the crystal phases per added PNC as,

$$V_{\text{PNC}} = \frac{V_{c,\text{final}}}{N_c}$$

and considering the total obtained product to be irrespective of the framework composition and density,  $V_{\text{PNC}}$  reflects the average increase of solid volume per condensed PNC. In terms of already present crystal volume,  $V_c(t) = V_{\text{PNC}}(N_0 - N(t))$ , the probability that at time  $t$  one of the  $N_c$  PNCs in the final crystals has already crystallised, can thus be expressed as:

$$P(t) = \frac{V_c(t)}{N_c V_{\text{PNC}}}$$

The formed crystal volume consists of all crystals present at time  $t$ . The volume of a single growing crystal,  $\varphi$ , is a cubic function of its characteristic radius, multiplied with a geometric factor  $\vartheta$  (*e.g.*  $4\pi/3$  for a sphere or 1 for a cube),

$$\varphi = \vartheta r^3$$

A crystal nucleated at time  $\tau$ , which increases its radius in time, with a function  $g(t, \tau)$  describing the temporal evolution of the crystal radius yields the volume of a crystal born at  $\tau$ , as a function of time,

$$\varphi(t) = \vartheta [g(t, \tau)]^3$$

Defining  $j(\tau)$  as the nucleation rate, the crystal volume arising from all crystals nucleated at  $\tau$  in an interval  $[\tau, \tau + \Delta\tau]$  is:

$$\phi(t, \tau, \Delta\tau) = j(\tau)\Delta\tau\vartheta[g(t, \tau)]^3$$

The probability that a PNC within  $N_c$  is already part of any crystal nucleated in  $\Delta\tau$ , therefore relates to the fraction of  $N_c$  in  $\phi(t, \tau, \Delta\tau)$ ,

$$P(t, \tau, \Delta\tau) = \frac{\phi(t, \tau, \Delta\tau)}{N_c V_{\text{PNC}}}$$

The total probability for crystallised PNC, is the product of probabilities for all possible  $\Delta\tau$ :

$$P_{\text{crystal}}(t, \tau) = \prod_{\text{all } \Delta\tau} \left[ \frac{\phi(t, \tau, \Delta\tau)}{N_c V_{\text{PNC}}} \right] = \exp \left[ \sum_{\text{all } \Delta\tau} \ln \left[ \frac{\phi(t, \tau, \Delta\tau)}{N_c V_{\text{PNC}}} \right] \right]$$

Expansion of the logarithm leads to,

$$P_{\text{crystal}}(t, \tau) = 1 - \exp \left[ \sum_{\text{all } \Delta\tau} - \frac{\phi(t, \tau, \Delta\tau)}{N_c V_{\text{PNC}}} \right]$$

If nucleation is instantaneously occurring during a time interval  $\Delta\tau$  at  $\tau = 0$ , *i.e.* only occurring at the start of crystallisation, and being rapidly exhausted afterwards,  $P_{\text{crystal}}(t, \tau)$  can be approximated by:

$$P_{\text{crystal}}(t, \tau) = 1 - \exp \left[ - \frac{n_\phi \vartheta(g(t))^3}{N_c V_{\text{PNC}}} \right],$$

with  $n_\phi$  being the number of nuclei formed in an induction period  $\tau$ . In the case of continuous random nucleation, the summation is transformed into an integral,

$$P_{\text{crystal}}(t) = 1 - \exp \left[ \sum_{\text{all } \Delta\tau} \left[ -j(\tau)\Delta\tau \frac{\vartheta[g(t, \tau)]^3}{N_c V_{\text{PNC}}} \right] \right] \xrightarrow{\Delta\tau \rightarrow 0} 1 - \exp \left[ - \frac{\vartheta}{N_c V_{\text{PNC}}} \int_0^t j(\tau)[g(t, \tau)]^3 d\tau \right]$$

This distribution function resembles the often used JMAK approach, which is based on a statistical model derived in 1937 by Kolmogorov, to specifically describe volume to volume transformations from liquid to solid, or solid to solid state, *e.g.* crystallisation of glass.<sup>22</sup> However, in the present case, incongruent transformation of only a fraction of the initial system with different composition of solid and liquid phase is considered. The possibility to use similar statistics in both cases is rooted in the fast liquid dynamics and kinetics in the homogeneous liquid phase, compared to the surface processes. Furthermore, assuming a large and constant liquid volume, no troublesome impingement of nucleating crystals needs to be considered as the crystal volume is formally not part of the liquid volume.

**3.2.3 Model of surface reactions.** The first test for the derived kinetic model is the option to fit it to the measured data, which requires a radial growth function  $g(t, \tau)$ . Such a function can be obtained from the kinetics of the surface reactions,



if known. The measurement principle, as well as the statistical model focus on the increase of zeolite product with time. Therefore, the suggested surface reactions also emphasise growth reactions, in a first approach ignoring surface dissolution. Fast dynamics in the liquid phase during nucleation and growth, defined as a prerequisite for derivation of the statistic model, imply the surface processes are rate-limiting and determine the increasing product fraction. We first derive rate laws for our proposed surface reactions and then discuss these in view of radial growth  $g(t, \tau)$ , to deduce which analytical forms  $P_{\text{crystal}}(t)$  can take. Fast liquid-phase dynamics ensure identical PNC concentration at each point and time within the growth medium, also when a liquid volume is in contact with any growing crystal. The radial growth rate of the surface must be related to the number of crystallised PNC per time and area. In the herein studied system the pre-nucleation clusters consist of aluminosilicate oligomers, ion-paired to alkalis. PNCs react with the surface by nucleophilic substitution, releasing alkali cations, and hydroxide ions as leaving groups into the liquid volume. In a liquid supersaturated with PNC, this process can be described by a precipitation dissolution equilibrium, followed by the release of MOH from the surface (Fig. 4).

Two cases need to be considered for determination of the rate laws. In the case of fast MOH desorption ( $k_d \gg k_r, k_{-r}$ ), the transition of liquid-state PNC to the active surface state,  $\overline{(\text{C-PNC})^* \text{MOH}}$ , is growth rate-limiting, indicating a steady state approximation of the crystal growth rate:

$$\frac{d\text{PNC}}{dt} = -k_r \text{PNC} + k_{-r} \overline{(\text{C-PNC})^* \text{MOH}}$$

$$\overline{(\text{C-PNC})^* \text{MOH}} = \frac{k_r}{k_{-r} + k_d} \text{PNC}$$

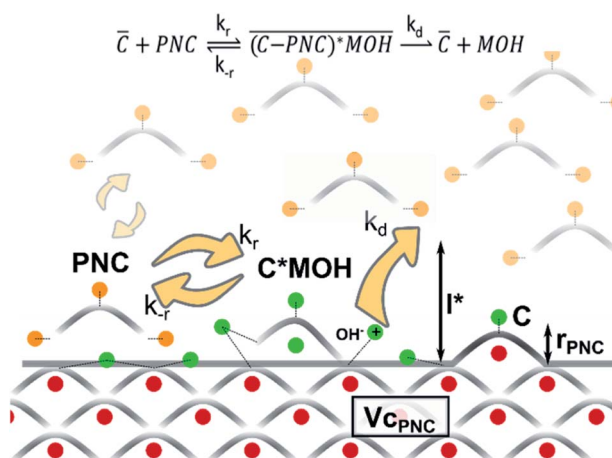


Fig. 4 Suggested mechanism of growth reactions. PNC are in equilibrium with the liquid. Once attached to the surface, the formed cation and hydroxide (not shown) have to move to a distance  $l > l^*$  from the surface to prevent re-dissolution. Also shown: volume taken by 1 PNC in the solid ( $V_{\text{PNC}}$ ) and added height per attached PNC ( $r_{\text{PNC}}$ ). The active surface state  $\overline{(\text{C-PNC})^* \text{MOH}}$  is symbolised by C\*MOH. Circles represent cations attached to PNC (grey bows) in liquid volume (orange), growing surface (green) and crystal (red).

$$\frac{d\text{PNC}}{dt} = \left( -k_r + k_{-r} \frac{k_r}{k_{-r} + k_d} \right) \text{PNC}$$

$$k_d \gg k_r, k_{-r} : \frac{d\text{PNC}}{dt} \approx -k_r \text{PNC}$$

$$\text{PNC} \propto \exp(-k_r t)$$

When desorption is slow and rate-limiting, the surface states are in equilibrium with liquid-state PNC, as defined by the formal solubility product,  $K_{sp} = k_{-r}/k_r$ . With the pre-equilibrium approximation, the rate of growth is determined by  $k_d$ ,

$$-\frac{d\text{PNC}}{dt} = k_d \overline{(\text{C-PNC})^* \text{MOH}} = k_d \frac{1}{K_{sp}} \text{PNC}$$

To dissolve  $\overline{(\text{C-PNC})^* \text{MOH}}$  back into the liquid as PNC, a nucleophilic attack by the hydroxide ion on the formed siloxane bond is necessary. Therefore, the rate of dissolution is linked to the mobility of MOH in the system. Considering preservation of local charge neutrality, the hydroxide moves with the cation, so that the cation mobility determines the rate of crystallisation. Therefore, the reaction  $\overline{(\text{C-PNC})^* \text{MOH}} \rightarrow \text{C} + \text{MOH}$  is defined by a rate that reflects the time needed to remove  $\text{M}^+$  from the site of condensation by a critical distance  $l^*$ . In a first approximation, the cation mobility in the system can be described as a random change of coordination partners, *i.e.* the negative charges on the liquid-state oligomers and on the growing surface. With assumption 1, a constant concentration of cations in the growth medium, an average distance for each ligand switch and an average residence time with each partner can be presumed. Such a process is closely related to chemical exchange. In this picture, the cation mobility can be described as a random walk with a hopping rate  $D$ , related to the square of the average step distance, which depends on the interaction strength between cation and ligand. The probability that a freshly condensed PNC still resides on the surface ( $0 < x < l^*$ ) after a time  $t$ , is obtained by integration of the probability distribution function describing the random walk process,

$$dP(x, t) = \frac{d\overline{(\text{C-PNC})^* \text{MOH}}(x, t)}{\overline{(\text{C-PNC})^* \text{MOH}}} = \frac{1}{\sqrt{\pi Dt}} \exp\left(-\frac{x^2}{4Dt}\right) dx dt$$

Integration for  $x$  in the limits 0 to  $l^*$ , using the expanded error function, results in the probability function,

$$dP(t) = \frac{d\overline{\text{C}^* \text{MOH}}}{\overline{\text{C}^* \text{MOH}}} \approx \frac{l^*}{\sqrt{\pi Dt}} dt$$

Considering fast dynamics compared to sampling times, only the first term of the expansion is kept since the standard deviation of the Gaussian distribution ( $\sigma = 4Dt$ ) is large compared to  $l^*$ . This probability function reflects the changing number of active surface states resulting from MOH release. Therefore, the radial growth rate is related to,

$$\frac{d\text{PNC}}{dt} = \text{PNC} \frac{-l^*}{K_{\text{sp}}\sqrt{\pi Dt}}$$

$$\text{PNC} \propto \exp k_d/K_{\text{sp}}\sqrt{t}$$

To derive the global evolution of solid product,  $P_{\text{crystal}}(t)$ , a function  $g(t, \tau)$  has been introduced, describing the crystal radius at time  $t$  for a crystal nucleated at  $\tau$ . In the following section, the derived surface reactions are linked to  $g(t, \tau)$  for the cases of steady-state and pre-equilibrium conditions.

**3.2.4 Model of conductivity data.** The attachment of a PNC on a surface element of a crystal with radius  $r$  leads to a radius increase by the average height of a PNC in the crystal in the growth direction,  $r_{\text{PNC}}$  (Fig. 4). For crystal nucleation at time  $\tau$  and a crystal growth time of  $(t - \tau)$ , the crystal radius increase depends on  $g(t, \tau)$ . When step 1 of the surface processes (Fig. 4 and 6) is rate-limiting (steady-state approximation), this results in a crystal growth rate of,

$$g_{\text{r}}(t, \tau) = r_{\text{PNC}}(\text{PNC}(\tau) - \text{PNC}(t)) \propto r_{\text{PNC}}(e^{-g\tau} - e^{-gt}) \approx r_{\text{PNC}}k_{\text{r}}(t - \tau)$$

If the growth is limited by the desorption of MOH from the crystal surface (Fig. 4 and 6), the resulting crystal growth rate  $g_{\text{d}}(t, \tau)$  becomes,

$$g_{\text{d}}(t, \tau) = r_{\text{PNC}}(\text{PNC}(\tau) - \text{PNC}(t)) \propto r_{\text{PNC}} \left( e^{-k_{\text{d}}\sqrt{t}} - e^{-k_{\text{d}}\sqrt{\tau}} \right) \approx r_{\text{PNC}}k_{\text{d}}(\sqrt{t} - \sqrt{\tau})$$

Therefore, the probability of PNC crystallisation,  $P_{\text{crystal}}(t, \tau)$ , can be determined for the two limiting cases, assuming a nucleation rate of the form  $j(\tau) = J\tau^y$ ,

$$P_{\text{crystal}}(t, \tau) = 1 - P_{\text{crystal}}(t) = 1 - \exp \left[ - \frac{J\vartheta(r_{\text{PNC}}k)^3}{N_{\text{c}}V_{\text{PNC}}} \int_0^t \tau^y [(t^x - \tau^x)]^3 d\tau \right]$$

with  $x = 1$  and  $k = k_{\text{r}}$  for surface reaction limitation, and  $x = 1/2$  and  $k = k_{\text{d}}$  in the case of desorption limitation. Assuming a constant nucleation rate upon reaching crystallisation conditions ( $\tau = 0$ ), integration yields

$$P_{\text{crystal}}(t) = 1 - \exp \left[ - \frac{J\vartheta(r_{\text{PNC}}k_{\text{r}})^3}{N_{\text{c}}V_{\text{PNC}}} t^{3x+y} \left( \frac{1}{y+1} - \frac{3}{x+y+1} + \frac{3}{2x+y+1} - \frac{1}{3x+y+1} \right) \right] = 1 - \exp[-G_{\text{n}}t^{3x+y}]$$

In the case of instantaneous nucleation, terminated before crystal growth proceeds,  $P_{\text{crystal}}(t)$  can be expressed as:

$$P_{\text{crystal}}(t) = 1 - \exp\left[-\frac{n_{\phi}\vartheta t^{3x}}{N_c V_{\text{PNC}}}\right] = 1 - \exp[-G_{\text{in}} t^{3x}]$$

For the here studied systems, crystal growth occurs by the addition of pre-nucleation clusters consisting of aluminosilicate-oligomers ion-paired to alkalis. Growth proceeds by siloxation reactions under release of the corresponding ion-paired cations and hydroxide into the medium. The charge release into the synthesis liquid, driven by the condensation of PNC as a function of time, can therefore directly be related to the derived distribution function,

$$P_{\text{crystal}}(t) = \frac{\text{solid product}(t)}{\text{total solid product}(t_{\text{final}})} = \frac{\sigma(t) - \sigma(t_0)}{\sigma(t_{\text{final}}) - \sigma(t_0)}$$

The derived probability as a function of time can take the form,

$$P_{\text{N}}(t) = 1 - \exp[-Gt^z]$$

All conductivity data could be described with such a function, suggesting the derived model indeed describes crystal growth as shown in Fig. 3. The fits along with their residuals are supplied in Fig. S4.† The conductivity curve is determined by two parameters, being the exponent, and multiplication factor of the variable time. The former indicates the radial growth of the crystals and the absence or presence of a nucleation rate. The latter contains the rate constants  $G_{\text{in}}$  and  $G_{\text{n}}$  accounting for growth and initially present nuclei or a combination of growth and nucleation for the scenarios of instantaneous *vs.* constant nucleation, respectively. As shown in Fig. 3, where the lines represent the fit of the data, the derived model is in excellent agreement with experimental conductivity data. The derived exponents (Fig. 5) do not significantly vary for the same cation with temperature, a clear indication that the global mechanism did not change. The slight variation of  $z$  for sodium with temperature will be addressed later in this article. Furthermore, the growth constants  $G$  show approximately linear behaviour in an Arrhenius plot, which indicates the rate-limiting steps are thermally activated processes, respecting the Boltzmann distribution, valid for surface condensation (step 1) as well as for chemical exchange (step 2). Therefore,  $G$  is linked to the activation energies for surface condensation, when reaction-limited, or the cation–ligand interaction strength for desorption limitation.

If the surface reactions suggested in 3.2.2 describe the surface growth and the reaction kinetics do not change during growth, then  $x$  can either take a value of  $x = 1$ , for reaction limitation, or  $x = 1/2$  for desorption limitation. Therefore, the experimentally determined exponent  $z$  takes the form  $z = 3 + y$  for the former, and  $z = 3/2 + y$  for the latter. If constant or instantaneous nucleation is considered as limiting cases, this means any exponent  $z$  must either be between  $3 < z < 4$  or  $3/2 < z < 5/2$ , respectively. Comparing these values to the experimentally obtained parameters, it is concluded that crystallisation in the sodium-containing systems proceeds with  $z \sim 3/2$ , and zeolite growth is controlled by the desorption of MOH from the growing surface ( $x = 1/2$ ). Nucleation is quickly exhausted, *i.e.*  $y$  is small

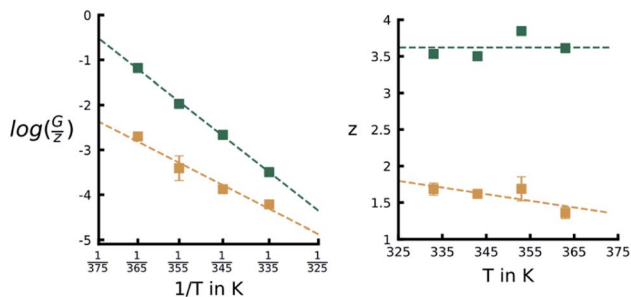


Fig. 5 Fitting parameter trends as given by an Arrhenius plot of the growth constant,  $G$ , and the determined values for the exponent,  $z$ . The values for Cs and Na are given in green and yellow, respectively.

or zero ( $y \sim 0$ ). Therefore, the crystal surface is observed to be in (meta)equilibrium with the growing surface. In the case of Cs as the counterion, the experimental value for  $z$  is close to  $z \sim 4$ , the maximum value possible for the here proposed growth and surface processes, implying quasi-constant nucleation over the whole crystallisation process. In this case, zeolite growth is limited by the surface reaction ( $x = 1$ ) and MOH release is so fast that no equilibrium between the liquid and the solid surface can be established.

## 4. Discussion

### 4.1 Model justification and rationale

The surprisingly good agreement with the predicted exponents for surface reaction limitation and constant nucleation for Cs ( $x = 1, y \sim 1$  and  $z \sim 4$ ), and MOH desorption limitation for Na ( $x = 1/2, y \sim 0$ , and  $z \sim 3/2$ ) strongly suggests the proposed model, despite extensive simplification, adequately describes the here observed kinetics of zeolite crystallisation (Fig. 6). This model directly relates the state of the liquid to the growing surface and increasing crystal volume. It needs to be pointed out that the derived model is necessarily incomplete because it only accounts for the global increase of zeolite product.

Considering the combination of a fairly invariable liquid phase speciation, fast liquid state dynamics and low number density of hydroxide ions in the system, a critical distance for irreversible removal of the hydroxide leaving group from the active surface state can be introduced. At this distance, a nucleophilic attack by the hydroxide will occur on liquid-state species, rather than on the active surface state (Fig. 4 and 6). Therefore, reversing the second step in the reaction mechanism would require generation of a free hydroxide in the liquid phase at a distance to the surface closer than  $l^*$ . As removal of a fully incorporated growth unit would imply multiple of these unlikely de-siloxation events, the model only considers the initial, most important, siloxation in step 1 (Fig. 6). Attachment on the surface with multiple bonds and the option that a PNC can be optimised according to the growing surface structure is not explicit in the proposed model. However, once a PNC is irreversibly attached by the first removal of MOH, any following reorganisation and/or surface siloxation can be assumed to be fast, so that the kinetics should remain dominated by  $k_r$  and  $k_d$ .

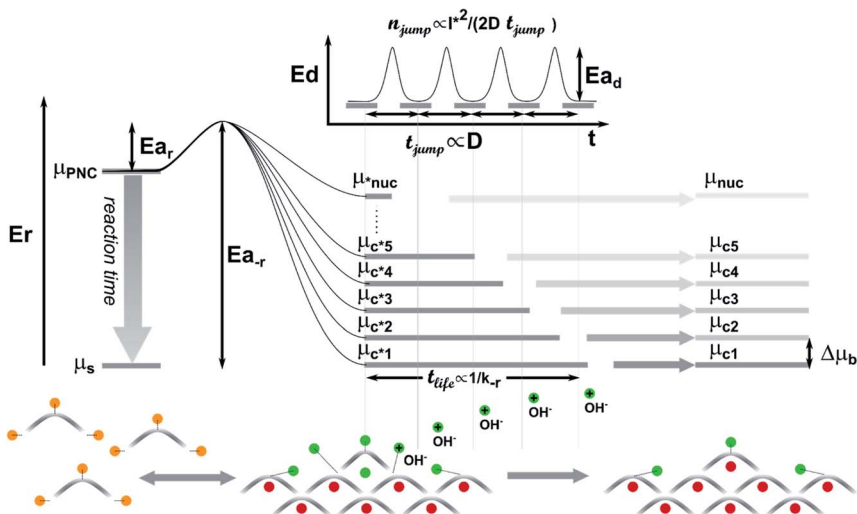


Fig. 6 Illustration of energetics and timeline of proposed surface reactions. Supersaturated liquid state PNC (left) has a chemical potential  $\mu_{\text{PNC}} > \mu_s$  and condenses on the surface upon thermal activation by  $Ea$ . Consumption of PNC results in lowering its energy until saturation is reached  $\mu_{\text{PNC}} > \mu_s$ . The different active surface states  $C_i^*$  (middle), have energies  $\mu_{c^*i}$ , ( $\mu_{\text{nuc}}$  indicates the energy of a PNC in emerging nucleus), which determines the lifetime  $t_{\text{life}}$  of  $C_i^*$ . Cation and hydroxide generated in the condensation need to be removed to consolidate  $C_i^*$  into the final crystal C (right). This process is related to the chemical exchange rate of the cation (green circle), characterised by activation energy  $Ea_d$ . Note that (C-PNC)\*MOH cations that will be included as extra-framework cations (red circles) still participate in chemical exchange, driven by  $Ea_d$ . After  $n_{\text{jump}}$  of the cation, the associated hydroxide is no longer available to return  $C^*$  to PNC. If  $t_{\text{life}}$  of  $C_i^*$  is larger than it takes the cation to perform  $n_{\text{jump}}$ , the active surface state turns into crystal, or else the attached PNC returns to the liquid.

Upon association of a PNC with the growing crystal surface, generation of the initial bond between surface and PNC also generates a hydroxide ion. In the first approximation, the activation energy (Fig. 6,  $Ea_r$ ) for this reaction, yielding the intermediate  $(\text{C-PNC})^*\text{MOH}$ , should be similar, if not identical to siloxation reactions in the liquid. This assumption is justified by the reversible and fast bond breaking and making, needed for (meta)-equilibration in the liquid, a prerequisite to allow the derivation of the statistical model. The backwards reaction  $(\text{C-PNC})^*\text{MOH} \rightarrow \text{PNC}$ , re-dissolving the active surface state, however, requires activation energy  $Ea_{-r}$ , the sum of  $Ea_r$  and the gain in energy  $\Delta\mu_{C^*} = \mu_{\text{PNC}} - (\mu_s + \mu_{C^*})$  (Fig. 6). In the case of high PNC supersaturation, *i.e.* high aluminate content in the liquid, the chemical potential ( $\mu_{\text{PNC}}$ ) of PNC is high, resulting in a high activation energy ( $Ea_{-r}$ ) for the backwards reaction. Consequently, the lifetime ( $t_{\text{life}}$ ) of  $(\text{C-PNC})^*\text{MOH}$  is high compared to the time needed to remove the generated hydroxide to a distance  $l^*$ , inhibiting the backward reaction (Fig. 6).

This second step,  $(\text{C-PNC})^*\text{MOH} \rightarrow \text{C} + \text{MOH}$ , was modelled as a function of the average interaction time between a cation and its coordination partner in the ion pairs. This process is related to the random walk continuously occurring in the system, where cations jump between coordination partners. Each jump involves breaking the existing bond between cation and coordination partner,

reforming a similar bond with the next partner. This occurs with a hopping rate  $D$  and associated activation energy ( $E_{a,d}$ ), characteristic for the cation type in the growth medium. Given that the nucleophilic attack of the hydroxide ion is needed to re-dissolve PNC from the surface, the hopping rate  $D$  of a cation in the growth medium decides on the (ir)reversibility of PNC attachment to the growing crystal. If cation hopping is slow, because interaction energy with partners is high, removal of hydroxide is slow. The resulting long residence time of  $\overline{(\text{C-PNC})^* \text{MOH}}$  allows reversal of the PNC attachment to the surface by the pre-equilibrium. Only long-lived surface sites, with high stability and long lifetime ( $t_{\text{life}} > n_{\text{jump}} \times t_{\text{jump}}$ , Fig. 6) can transform into crystallised material.

During crystallisation, PNC will be consumed, until the concentration reaches the solubility and the PNC energy in the liquid is equal to  $\mu_s$  (Fig. 6). The closer  $\mu_{\text{PNC}}$  approaches  $\mu_s$ , the higher the rates of the re-dissolution of the surface sites become, and the more strongly their respective energy differences will affect their relative lifetimes. PNC concentration should however not affect the intrinsic cation hopping frequency, so that the time to remove cation and hydroxide from  $\overline{(\text{C-PNC})^* \text{MOH}}$  should remain largely unaffected. Therefore, supersaturation should not affect the time needed to make an active surface state a part of the crystal. This implies, that for low supersaturation levels and slow cation dynamics, those surface condensation sites with the lowest energy will be preferred, leading to increasingly faceted crystals of the most stable crystal phase throughout the reaction. On the other hand, when the cation is extremely mobile, *i.e.* only weakly interacting, then  $\overline{(\text{C-PNC})^* \text{MOH}}$  changes into a crystal almost as soon as it is formed, and the resulting crystal shape should have an isotropic, spherical character.

As is evident from the Arrhenius plots in Fig. 5, all crystallisation processes proceed faster with increasing  $T$ , because all reactions ( $k_r$ ,  $k_{-r}$  and  $k_d$ ) are thermally activated processes. Furthermore, temperature also affects the supersaturation, because of temperature dependency of the solubility of the solid phases.<sup>20</sup> This readily explains obeisance or ignorance of the Ostwald step rule, as the latter only can be followed when the possible surface states on all solid phases can achieve (quasi)equilibrium distribution. In other words, a dissolution–reprecipitation process can only proceed when the dissolution reaction ( $k_{-r}$ ) is not inhibited by the second reaction step. Therefore, one should expect more prominent facets at higher  $T$ , and increasing fractions of the thermodynamically more stable phases for slow cation dynamics, as observed for the Na system.

## 4.2 Nature of cations

All results point to the critically important role of the cation in zeolite crystallisation from homogeneous, highly ionic media. The cation is involved in finalising the individual pre-nucleation cluster attachment by removal of the hydroxide nucleophile from the surface and inhibiting immediate re-dissolution. On a chemical level, Na and Cs cations strongly differ. Sodium is a small, kosmotropic cation and is highly stable in a hydrated state. It only forms ion pairs with (alumino)silicate oligomers, in the absence of or with limited water molecules or other favourable ligands.<sup>21</sup> Cesium, on the other hand, is a large chaotropic cation, known to weakly interact with water, and even less with hard charges. This difference is well-known,<sup>24,25</sup> and reflects the affinity for oxygen ligands. The hydration energy of the cations can serve as a measure of

oxophilicity. For  $\text{Na}^+$  and  $\text{Cs}^+$ , hydration energies of 409 vs. 264  $\text{kJ mol}^{-1}$  are reported.<sup>26</sup> This marked contrast also results in vastly different ionic mobility in water, where sodium moves very slowly, compared to cesium (50 vs. 77  $\text{m}^2\text{S mol}^{-1}$ ).<sup>27</sup> Admittedly, aqueous solutions are not an ideal comparison for the here discussed hypohydrated ionic liquids. Nonetheless, similar principles of cation mobility should apply. Microscopically, the alkali-cations, with low covalent bonding character, move through the medium, while changing available coordination partners. In aqueous systems, this is a function of the average residence time of water molecules next to the cation. This time is one order of magnitude larger for Na than for Cs.<sup>28</sup> Interestingly, the here measured ratio between conductivities in Na and Cs systems is similar to the ratio of reported ionic mobilities of  $\text{Na}^+$  and  $\text{Cs}^+$  (Table S2†). The observed conductivity is mainly driven by the mobility of  $\text{Na}^+$  and  $\text{Cs}^+$ , because hydroxide ions are mostly depleted. Therefore, the conductivity of comparable ionic liquids reflects the mobility of the cations. In view of this, it is no surprise that the cation migration from the surface of the growing zeolite is rate-limiting in the case of sodium, but not for cesium, even though direct experimental data for chemical exchange rates are not yet available.

### 4.3 Topology and morphology of products

Inspecting the morphology of the obtained zeolites, a number of observations can readily be explained. In the case of Cs, many small unfaceted, almost perfectly spherical crystals are obtained. The proposed model predicts such crystal morphology based on a continued nucleation and indiscriminate PNC attachment, ( $y = 1, x = 1; z = 4$ ). Both imply the energy of  $(\text{C-PNC})^*\text{MOH}$  on the crystal surface is much lower compared to its ion-paired liquid state, PNC, which also is reflected in a very low solubility and a high yield. Therefore, it is concluded, that the initial supersaturation in the studied Cs-systems is always extremely high, and/or the mobility of Cs in the medium is very fast in comparison. Both should lead to many small spherical crystals.

For Na, very different conclusions can be drawn. The exponent close to  $z \sim 3/2$  indicates that the transport of the cation from the surface is rate-limiting. PNC attachment and dissolution is fast and reversible, in comparison. The obtained large crystals are faceted and different zeolite phases are observed during the crystallisation, with the most stable GIS dominating at higher temperatures. This suggests that the energy of the liquid-state PNC is close to its energy on the surface(s), which enables faceted crystals and obeisance of the Ostwald step rule, both gaining importance with increasing temperature.<sup>23</sup> The suggested growth model only accounts for the global increase of zeolite crystals. In accordance with modern nucleation theory, the first appearing solid should be the one where the energy difference between growth units in liquid and solid is the smallest.<sup>5</sup> This represents the solid with the lowest thermodynamic stability. Over time, this solid is then transformed into the thermodynamically more stable structure(s). In the case of Na, the initial formation of FAU is faster than for GIS, so the fraction of FAU is decreasing with crystallisation temperature. The general conclusion for sodium that the liquid-state energy of PNC ( $\mu_{\text{PNC}}$ ) is of the same order of magnitude as in the forming crystals, possibly also explains the slightly too high exponents observed at lower temperatures. Initially, at a given temperature the supersaturation is higher



so that nucleation should slow down with reaction time. Therefore, the possibility of decreasing continuing nucleation cannot be discounted, which leads to a higher number of smaller crystals and slightly increased exponents ( $x = 1/2$ ,  $0 < y < 1$ ), as observed at lower temperatures for sodium systems (Fig. 5).

In this work, the transition from Na-FAU to Na-GIS with increasing temperature is observed. While not studied *in situ*, high temperatures or extended crystallisation times lead to the formation of analcime, also with sodium. This allows direct comparison of the crystal morphology of Cs-ANA and Na-ANA formed at the same temperature. An experiment with a prolonged synthesis time of 1 week at 90 °C was performed for zeolite synthesis liquids in the presence of Na and Cs cations, both yielding the ANA framework. SEM images of the synthesized ANA zeolites (Fig. 7) indicate that even for a prolonged synthesis time, and for the synthesis of an identical zeolite framework, the crystal morphologies are highly dissimilar. As expected from the observed crystallisation kinetics, the formation of the ANA framework in the presence of sodium cations results in highly faceted crystals, indicating the active surface sites are sufficiently long-lived to achieve equilibrated populations, and the removal of NaOH from the surface is slow and rate-limiting. For Cs synthesis, even after a highly prolonged synthesis time (168 h instead of 4 h), when the liquid should have reached saturation, Cs-ANA crystals are still isotropic spheres, indicating comparably fast removal of CsOH. Following, these general conclusions will be put in perspective of generally accepted concepts of (zeolite) crystal growth.

While zeolite nucleation and growth is considered highly complex, Anderson *et al.* demonstrated that crystal growth, even of zeolites, needs to respect simple rules.<sup>29,30</sup> The surface of a growing crystal has a predictable energy landscape that can be explored *via* a unified three-dimensional partition model.<sup>29</sup> For a given zeolite framework, crystal growth can be approximated by partitioning the zeolite in its cage structures, mathematically represented by the natural tiles concept.<sup>31</sup> It needs to be stressed that these natural tiles do not necessarily relate to precursor structure and molecular processes on a growing crystal surface. Instead, the concept identifies the energy of different surface structures from the perspective of the growing surface.<sup>29</sup> As most stable and desirable structures, states with high connectivity are favoured, implying surface silicate or aluminate to be oxolated to three, in some cases two, neighbours. This directly results in closed tiles, present on the surface and requires each growth step to close the next set of tiles, as demanded by topology. This way, the topology of the zeolite defines a set of active

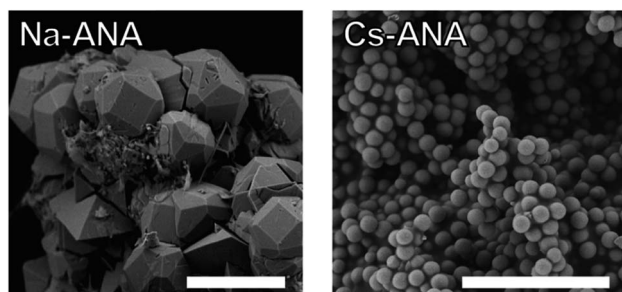


Fig. 7 SEM images of ANA zeolite, synthesized in the presence of Na<sup>+</sup> (Na-ANA) or Cs<sup>+</sup> (Cs-ANA). The white line represents 4  $\mu\text{m}$  in both picture frames.

surface states with differing energies, analogous to kinks, steps and terraces in the simple TLK model. Energy differences between these sites are defined as multiples of  $\Delta\mu_b$ . The CrystalGrowth software utility<sup>30</sup> explores the resulting crystal morphology based on kinetic Monte Carlo simulations, evaluating the crystal shape, entirely based on  $\Delta\mu_b$ , *versus* the supersaturation. In the case of low supersaturation,  $\Delta\mu_b$  is large in comparison, facets are expressed as precipitation and dissolution can occur with similar rates, preferring the most stable states. If supersaturation is high, the energetic differences between surface states are negligible, compared to the very high activation energy necessary for dissolution, and isotropic crystal morphology is predicted. Comparing our proposed model to the CrystalGrowth, it is obvious that we should obtain the same result of spherical growth, when initial supersaturation is very high, the energy differences between active surface states  $(\text{C-PNC})^*\text{MOH}$  is comparably small, and/or the cation dynamic in the system is fast.

CrystalGrowth simulations were performed for the observed majority phases, being the ANA, FAU and GIS topologies. Crystallisation parameters were varied to match the observed morphologies (Fig. 8). As expected, isotropic crystal growth, observed for all Cs-ANA cases irrespective of  $T$  and even crystallisation time, is predicted by CrystalGrowth for extremely low energy separations  $\Delta\mu_b$ . However,

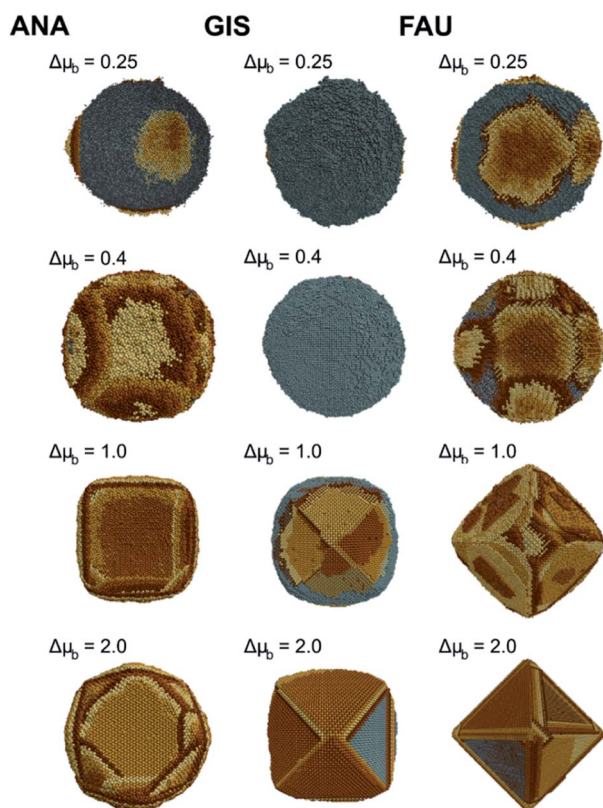


Fig. 8 Kinetic Monte Carlo simulations were performed in the CrystalGrowth software utility. Synthesis parameters were chosen to represent the observed crystal morphologies (details in ESI†). Values of  $\Delta\mu_b$  are given in  $\text{kcal mol}^{-1}$ .

even after very long crystallisation times, when supersaturation after initial solidification can be expected to be low, and  $\Delta\mu_b$  large in comparison, Cs-ANA still does not show any faceting. This can be explained with a very fast second crystallisation step because of the high mobility of Cs. Fast removal of the cation from the surface freezes a purely statistical distribution of active surface states. In the case of sodium, we always obtain faceted crystals, corresponding to large  $\Delta\mu_b$  in CrystalGrower, suggesting a low supersaturation throughout, and comparably slow cation dynamics. Considering, our proposed model reveals transport limitation for Na ( $x = 1/2$ ), the resulting morphology mirrors the (quasi)equilibrium distribution over the available surface sites as predicted by CrystalGrower for large  $\Delta\mu_b$ .

## 5. Conclusions

In summary, crystal nucleation and growth often displays behaviour that cannot be explained by classical nucleation theory.<sup>5,32</sup> Zeolite formation forms no exception.<sup>10</sup> In this work, we perform *in situ* conductivity measurements during zeolite synthesis from highly ionic homogeneous liquids. A suggested mechanism for the observed growth assumes ion-paired pre-nucleation clusters reversibly attach to and dissolve from the growing surface, only locked in place by desorption of metal cation and hydroxide removal. The cation release increases the conductivity of the synthesis liquid, which is directly accessible by state-of-the-art MEEIS.<sup>33,34</sup> A kinetic model of zeolite crystallisation was developed in excellent agreement with the measurements. This model proposes zeolite crystallisation can be limited either by the condensation of a pre-nucleation cluster on the surface or by transport of the resulting cation and hydroxide into the crystallisation medium. This model is verified by the variation of the alkali metal cation ( $\text{Cs}^+$  vs.  $\text{Na}^+$ ) present during crystallisation. The systems result in different zeolite topologies, but both can be described adequately, and reveal reaction limitation for the case of  $\text{Cs}^+$  and transport limitation for  $\text{Na}^+$ . Even though the suggested model is still very rudimentary, this success may be taken as an indication that with an improved version of the model and accurate measurement of zeolite growth rates, a generally valid description of zeolite growth might become possible.

## Conflicts of interest

There are no conflicts to declare.

## Acknowledgements

This work is funded by the bilateral FWO/FWF ZeoDirect project (I3680-N34), the Austrian COMET-K2 program, and FWO (1.5.061.18N and G083318N). This work received long-term funding from the Flemish Methusalem program and is funded by the European Research Council (ERC) under grant 371 agreement no. 834134 (WATUSO).

## Notes and references

- 1 J. J. d. Yoreo, Principles of Crystal Nucleation and Growth, *Rev. Mineral. Geochem.*, 2003, **54**, 57–93.

- 2 J. J. d. Yoreo, *et al.*, Crystallization by particle attachment in synthetic, biogenic, and geologic environments, *Science*, 2015, **349**, 498–508.
- 3 J. Baumgartner, *et al.*, Nucleation and growth of magnetite from solution, *Nat. Mater.*, 2013, **12**, 310–314.
- 4 G. Mirabello, *et al.*, Crystallization by particle attachment is a colloidal assembly process, *Nat. Mater.*, 2020, **19**, 391–396.
- 5 D. Gebauer, M. Kellermeier, J. D. Gale, L. Bergström and H. Cölfen, Prenucleation clusters as solute precursors in crystallisation, *Chem. Soc. Rev.*, 2014, **43**, 2348–2371.
- 6 D. Gebauer, A. Völkel and H. Cölfen, Stable Prenucleation Calcium Carbonate Clusters, *Science*, 2008, **322**, 1819–1822.
- 7 W. J. E. M. Habraken, *et al.*, Ion-association complexes unite classical and non-classical theories for the biomimetic nucleation of calcium phosphate, *Nat. Commun.*, 2013, **4**, 1507.
- 8 E. D. Dill, J. C. W. Folmer and J. D. Martin, Crystal Growth Simulations To Establish Physically Relevant Kinetic Parameters from the Empirical Kolmogorov–Johnson–Mehl–Avrami Model, *Chem. Mater.*, 2013, **25**, 3941–3951, DOI: 10.1021/cm402751x.
- 9 M. Fanfoni and M. Tomellini, The Johnson-Mehl- Avrami-Kohnogorov model: A brief review, *Il Nuovo Cimento D*, 1998, **20**, 1171–1182.
- 10 C. S. Cundy and P. A. Cox, The hydrothermal synthesis of zeolites: Precursors, intermediates and reaction mechanism, *Microporous Mesoporous Mater.*, 2005, **82**, 1–78.
- 11 M. J. van Vleet, T. Weng, X. Li and J. R. Schmidt, In Situ, Time-Resolved, and Mechanistic Studies of Metal-Organic Framework Nucleation and Growth, *Chem. Rev.*, 2018, **118**, 3681–3721.
- 12 R. M. Barrer, J. W. Baynham, F. W. Bultitude and W. M. Meier, Hydrothermal Chemistry of the Silicates. Part VIII, *J. Chem. Soc.*, 1959, 195–208.
- 13 D. W. Breck, Crystalline molecular sieves, *J. Chem. Educ.*, 1964, **41**, 678–689.
- 14 S. P. Zhdanov, Some Problems of Zeolite Crystallization, *Adv. Chem.*, 1971, **101**, 20–43.
- 15 E. M. A. Flanigen, Review and New Perspectives in Zeolite Crystallisation, *Adv. Chem.*, 1973, **121**, 119–139.
- 16 M. Kumar, M. K. Choudhary and J. D. Rimer, Transient modes of zeolite surface growth from 3D gel-like islands to 2D single layers, *Nat. Commun.*, 2018, **9**, 2129.
- 17 L. van Tendeloo, *et al.*, Zeolite synthesis in hydrated silicate ionic liquids, *Faraday Discuss.*, 2015, **179**, 437–449.
- 18 K. Asselman, *et al.*, Super-ions of sodium cations with hydrated hydroxide anions: inorganic structure-directing agents in zeolite synthesis, *Mater. Horiz.*, 2021, **8**, 2576–2583.
- 19 N. Pellens *et al.*, DOI: 10.1021/acs.chemmater.2c00418.
- 20 M. Houllberghs, *et al.*, Evolution of the crystal growth mechanism of zeolite W (MER) with temperature, *Microporous Mesoporous Mater.*, 2019, **274**, 379–384.
- 21 M. Hellström and J. Behler, Structure of aqueous NaOH solutions: insights from neural-network-based molecular dynamics simulations, *Phys. Chem. Chem. Phys.*, 2016, **19**, 82–96.

- 22 A. N. Kolmogorov, On the statistical theory of the crystallization of metals, *Bull. Acad. Sci. USSR*, 1937, **1**(3), 355–359.
- 23 M. Maldonado, M. D. Oleksiak, S. Chinta and J. D. Rimer, Controlling crystal polymorphism in organic-free synthesis of Na-zeolites, *J. Am. Chem. Soc.*, 2013, **135**, 2641–2652.
- 24 S. Koneshan, J. C. Rasaiah, R. M. Lynden-Bell and S. H. Lee, Solvent Structure, Dynamics, and Ion Mobility in Aqueous Solutions at 25 °C, *J. Phys. Chem. B*, 1998, **102**, 4193–4204.
- 25 R. M. Lynden-Bell and J. C. Rasaiah, From hydrophobic to hydrophilic behaviour: A simulation study of solvation entropy and free energy of simple solutes, *J. Chem. Phys.*, 1997, **107**, 1981–1991.
- 26 D. W. Smith, Ionic hydration enthalpies, *J. Chem. Educ.*, 1977, **54**, 540.
- 27 D. Lide, *CRC Handbook of Chemistry and Physics*, CRC Press, 96th edn, 2015.
- 28 L. Helm and A. E. Merbach, Water exchange on metal ions: experiments and simulations, *Coord. Chem. Rev.*, 1999, **187**, 151–181.
- 29 M. W. Anderson, *et al.*, Predicting crystal growth via a unified kinetic three-dimensional partition model, *Nature*, 2017, **544**, 456–459.
- 30 A. R. Hill, *et al.*, CrystalGrower: a generic computer program for Monte Carlo modelling of crystal growth, *Chem. Sci.*, 2020, **12**, 1126–1146.
- 31 V. A. Blatov, A. P. Shevchenko and D. M. Proserpio, Applied Topological Analysis of Crystal Structures with the Program Package ToposPro, *Cryst. Growth Des.*, 2014, **14**, 3576–3586.
- 32 S. Karthika, T. K. Radhakrishnan and P. Kalaichelvi, A Review of Classical and Nonclassical Nucleation Theories, *Cryst. Growth Des.*, 2016, **16**, 6663–6681.
- 33 N. Doppelhammer, *et al.*, Moving Electrode Impedance Spectroscopy for Accurate Conductivity Measurements of Corrosive Ionic Media, *ACS Sens.*, 2020, **5**, 3392–3397.
- 34 N. Doppelhammer, *et al.*, Using moving electrode impedance spectroscopy to monitor particle sedimentation, *IEEE Sens.*, 2021, **21**, 9636–9641.